Feasibility of Passively Autonomous Frequency Operations with APR1400

Dongju Choi, Yunseok Jeong, and Yonghee Kim*
Department of Nuclear and Quantum Engineering, Korea Advanced Institute of Science and Technology (KAIST), 291 Daehak-ro Yuseong-gu, Daejeon 34141, Republic of Korea
**Corresponding author: yongheekim@kaist.ac.kr*

***Keywords**: Passively Autonomous Frequency Operation, APR1400, KANT*

1. Introduction

The increasing penetration of variable renewable energy sources has led to significant challenges in maintaining frequency stability. Low-inertia systems experience larger and faster frequency excursions following disturbances, which increases the demand for flexible frequency control resources. At present, such frequency control capabilities are provided primarily by conventional synchronous generators (e.g., gas-fired and hydro units) and, increasingly, by battery energy storage systems, while nuclear power plants generally operate in base-load mode.

Conventional approaches to nuclear flexibility, such as scheduled load following, rely on the active control of reactor power through control rod movements and soluble boron adjustments. However, extending these active core control strategies to track the faster and more frequent power variations required for frequency response raises practical concerns. Continuous rod movement can cause excessive wear on the control rod drive mechanisms, potentially reducing the operational margin.

Passively autonomous frequency operation (PAFO) has been proposed to exploit the inherent self-regulation capability of the reactor core to circumvent these challenges [1]. In PAFO, variations in secondary-side heat removal induce changes in coolant and fuel temperatures, allowing inherent feedback to drive the core power toward a new equilibrium without active intervention. Recent studies have demonstrated that soluble-boron-free small modular reactors with strongly negative moderator temperature coefficients can provide primary and secondary frequency control in this purely passive manner [1].

Whether this PAFO philosophy can be extended to large-sized commercial PWRs like the APR1400 remains an open question. This paper evaluates the feasibility of PAFO in the APR1400 through three-dimensional whole-core transient analysis with an explicit steam generator model. Specifically, the research identifies the key physical constraints that govern PAFO performance across different burnup conditions.

2. Methods

2.1 Passively autonomous frequency operation

PAFO is a frequency regulation concept that enables reactor power adjustment without active reactivity control via control rods or soluble boron. Instead, power changes are induced passively through inherent reactivity feedback in response to variations in the core inlet coolant temperature, which are driven by changes in secondary-side heat removal [1].

During a frequency event, the demand power is reflected in the secondary-side control action through adjustments in the feedwater flow rate. This modifies the steam generator heat removal, leading to a change in the reactor coolant temperature at the core inlet. Owing to the negative moderator temperature coefficient, the resulting temperature change provides a passive reactivity change that shifts reactor power toward a new equilibrium consistent with the demand. The transient behavior is governed by the net reactivity feedback from the moderator, fuel, and xenon effects.

2.2 Reactor description

The analysis is performed for the standard APR1400 initial core. Since the design parameters, core configuration, and thermal-hydraulic characteristics of APR1400 are well documented in the literature, only a brief description is given here [2]. Two representative burnup conditions, at BOC (2 GWD/MTU) and EOC (18 GWD/MTU), are selected to account for burnup-dependent variations in feedback coefficients relevant to PAFO over the fuel cycle.

2.3 Computational code

The whole-core calculations are performed using a conventional two-step method with SERPENT2/KANT. Homogenized group constants are generated by the SERPENT2 continuous-energy Monte Carlo code with the ENDF/B-VII.1 library [3], and three-dimensional whole-core nodal calculations are carried out by the in-house KANT code based on a NEM/CMFD scheme coupled with thermal-hydraulics [4].

To represent primary-secondary interactions, a simplified steam generator model updates the core inlet coolant temperature T_{in} at each time step based on the power demand:

$$T_{in}^{k+1} = T_{in}^{k} - (T_{e,target}^{k} - T_{e}^{k}) \quad (1)$$

Here, $T_{e,target}^{k}$ is the core outlet temperature corresponding to the demanded power and T_{e}^{k} is the current outlet temperature. This treatment implicitly

assumes that the SG extracts thermal energy in accordance with the demand, allowing the inlet temperature to respond to load variations through passive feedback.

In addition to the simplified SG model, the U-Tube Steam Generator (UTSG) model is employed to explicitly capture the primary-secondary thermal interactions. The thermal hydraulics behavior of the UTSG is represented by the conservation equations of energy, mass and momentum as below,

$$\rho\frac{\partial h}{\partial t}+\frac{m}{A}\frac{\partial h}{\partial z}=\frac{Aq''}{V} \quad (2)$$

$$\rho\frac{\partial \rho}{\partial t}+\frac{\partial m}{\partial z}=0 \quad (3)$$

$$\frac{\partial m}{\partial t}+\frac{\partial}{\partial z}\left(\frac{m^2}{\rho}\right)=-\frac{\partial p}{\partial z}-\frac{fm|m|}{2D_e\rho}-\rho g\cos\theta \quad (4)$$

Here, symbols follow standard notation: ρ (density), h (enthalpy), m (mass flow rate), A (flow area), q (heat flux), V (control-volume), p (pressure), D_e (hydraulic diameter), f (friction factor), g (gravitational acceleration), and θ (tube elevation angle). Fluid properties are taken from steam tables, and pressure-drop and heat-transfer coefficients are computed using standard single- and two-phase correlations as functions of Reynolds number and flow regime [5].

As illustrated in Fig. 1, the reactor core and SG module are coupled through hot and cold leg transport delays. The thermal state of the primary coolant is exchanged between the two systems after accounting for their respective residence times. This coupling allows the core inlet temperature to reflect secondary-side power demand changes through the continuous circulation of the primary loop.

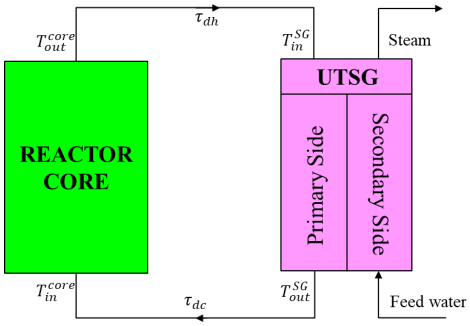

Figure 1 Schematic of coupling between the reactor core and steam generator

The transient calculation follows a sequential coupling scheme between the reactor core and the steam generator as illustrated in Fig. 2. At each time step, the neutronics module solves the time-dependent diffusion equations while the thermal-hydraulics module iteratively updates local parameters to incorporate the feedback until the convergence. Once converged, the updated core outlet temperature is transmitted to the steam generator after accounting for the transport delay of the hot leg. The UTSG module receives the demanded power as an input and iteratively solves the one-dimensional conservation equations for the primary and secondary sides until the heat transfer between the two systems is fully converged. Subsequently, the resulting SG outlet temperature is used to update the core inlet temperature after incorporating the cold leg transport delay, thereby providing the updated state for the subsequent time step as the integrated simulation continues throughout the transient.

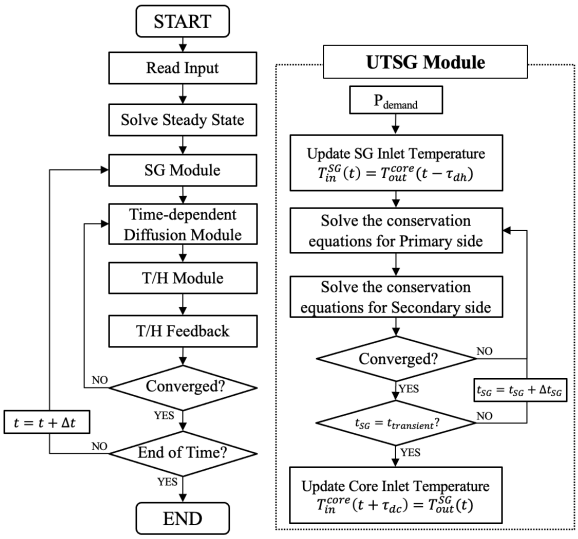

Figure 2 Flowchart of transient calculation and UTSG module in KANT

2.4 Frequency control scenarios

The frequency control scenarios are adapted from Abdelhameed et al. [1]. Two cases are considered: Primary PAFO (P-PAFO) for fast primary response (Table 1) and Secondary PAFO (S-PAFO) for slower secondary control and return-to-base-load behavior (Table 2). In both cases, the reactor starts from 100% rated power and switches from base-load to PAFO mode upon receiving grid frequency-control signals.

Table 1 Power scenario for primary frequency control

Step	Time (min.:sec.)	Power (%)	Ramp Rate (%P_r/sec.)
1	00:00 – 00:10	100	-
2	00:10 – 00:15	100 → 102.5	0.50
3	00:15 – 00:25	102.5 → 97.5	0.50
4	00:25 – 00:32	97.5 → 101	0.50
5	00:32 – 00:42	101 → 97.5	0.35
6	00:42 – 00:52	97.5 → 101	0.35
7	00:52 – 01:02	101 → 100	0.10
8	01:02 – 01:12	100 → 102.5	0.25
9	01:12 – 01:22	102.5 → 97.5	0.50
10	01:22 – 01:42	97.5	-
11	01:42 – 01:49	97.5 → 102.5	0.714

12	01:49 – 01:56	102.5	-
13	01:56 – 02:06	102.5 → 100	0.25
14	02:06 – 05:50	100	-

Table 2 Power scenario for secondary frequency control

Step	Time (min.:sec.)	Power (%)	Ramp Rate (%P_r/min.)
1	00:00 – 30:00	100	-
2	30:00 – 31:00	100 → 95	5
3	31:00 – 41:00	95	-
4	41:00 – 43:00	95 → 105	5
5	43:00 – 63:00	105	-
6	63:00 – 63:36	105 → 102	5
7	63:36 – 73:36	102	-
8	73:36 – 74:36	102 → 97	5
9	74:36 – 94:36	97	-
10	94:36 – 96:12	97 → 105	5
11	96:12 – 106:12	105 → 95	1
12	106:12 – 116:12	95 → 105	1
13	116:12 – 126:12	105	-
14	126:12 – 127:12	105 → 100	5
15	127:12 – 150:00	100	-

3. Numerical Results

3.1 Primary-PAFO

Figures 3 and 4 summarize the P-PAFO results at BOC. Figure 3 shows that the feedwater flow rate to the UTSG is adjusted in response to the demand power. Figure 4 compares the transient responses obtained with the UTSG and a simplified SG model, where “Approx” in the legend refers to the simplified SG model results.

With the simplified SG model, reactor power closely tracks the demand because the model effectively neglects transport delay and dynamic lag in the secondary-side thermal response. In contrast, the UTSG case shows a clear tracking delay in reactor power. This is expected because P-PAFO requires second-scale power adjustments, whereas the UTSG dynamics introduce time delay and thermal inertia that slow the propagation of secondary-side variations to the core inlet temperature. The turbine thermal power still follows the demand closely, which is consistent with the secondary side releasing or absorbing stored thermal energy while the core response lags.

In the UTSG case, the core inlet coolant temperature remains within the reactor coolant system (RCS) design limit [6], as shown in Fig. 4. The axial shape index (ASI) remains nearly constant during the transient, and the small ASI variation is attributable to minor changes in the core temperature profile induced by the inlet temperature perturbation. Notably, this constraint is satisfied at BOC even with a less negative MTC of −11.5 pcm/K, indicating that the secondary-side thermal buffering can maintain inlet-temperature compliance while enabling passive power adjustment.

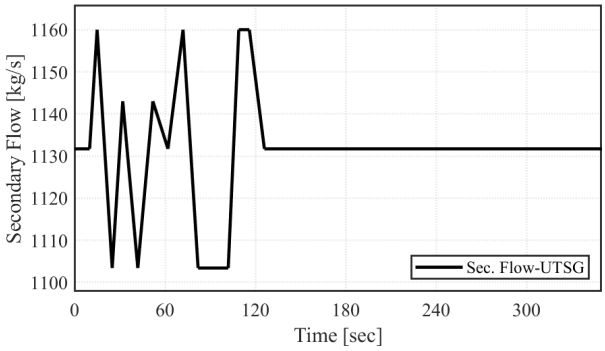

Figure 3 Feedwater flow rate variation during P-PAFO at BOC

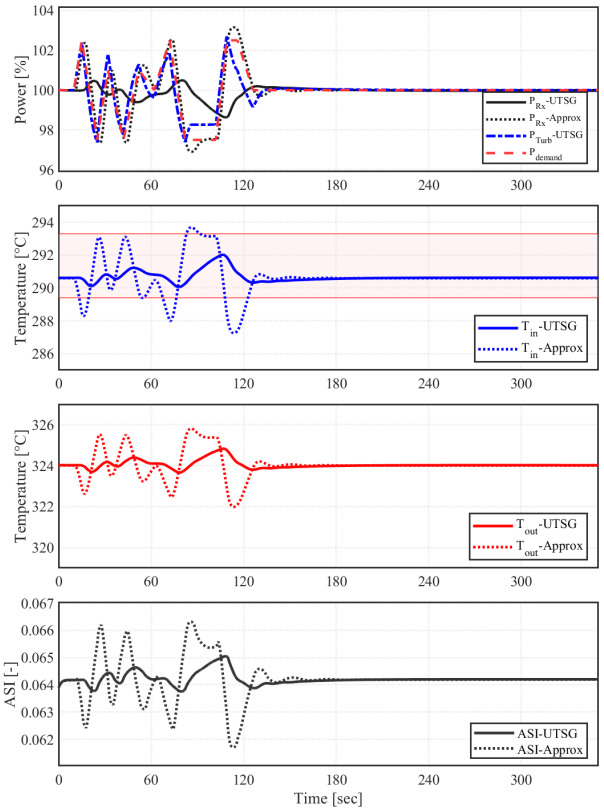

Figure 4 Simulation results of P-PAFO at BOC

Figure 5 presents the P-PAFO results at EOC. At EOC, the MTC is significantly more negative (−51.4 pcm/K) than at BOC. As a result, even with the transport delay imposed by the UTSG dynamics, the reactor power responds more strongly and approaches the demand trajectory more closely than in the BOC case.

Since the objective of primary frequency control is fast stabilization rather than perfect power tracking, these results suggest that PAFO can be feasible for the APR1400 initial core.

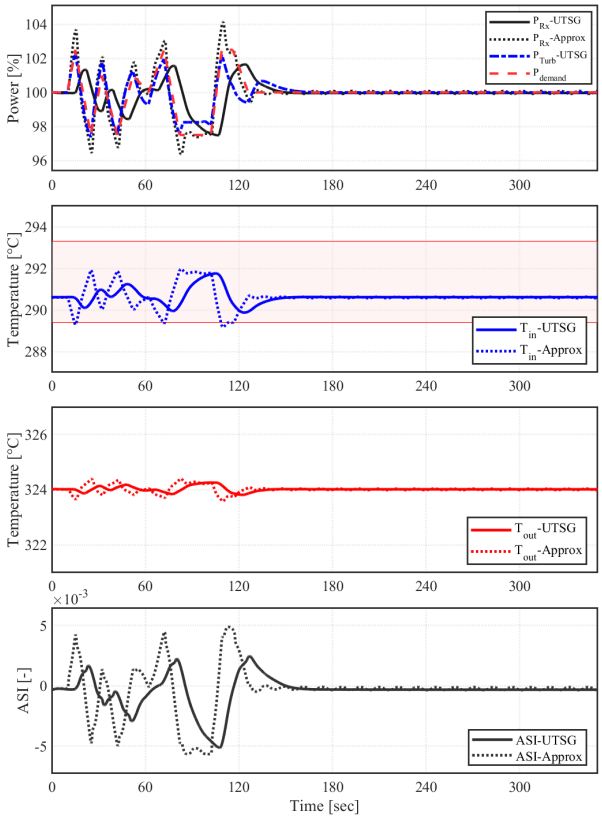

Figure 5 Simulation results of P-PAFO at EOC

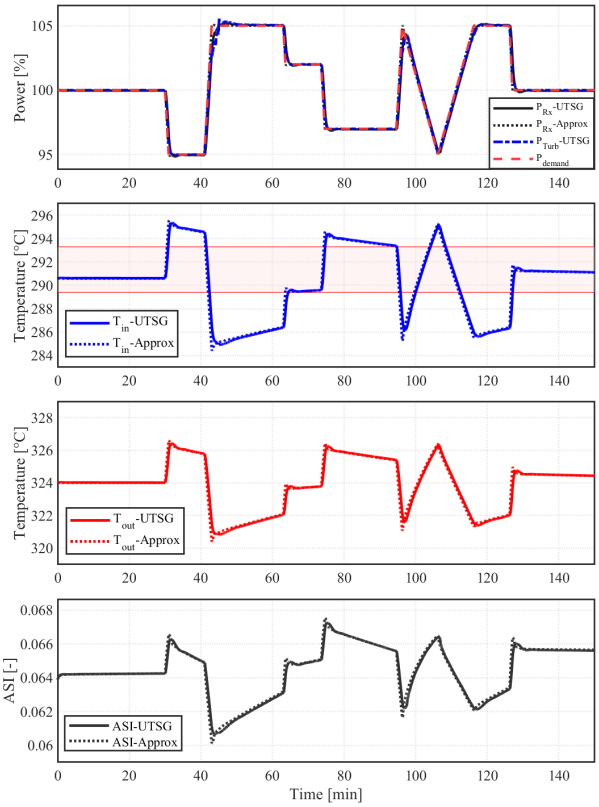

Figure 6 Simulation results of S-PAFO at BOC

3.2 Secondary-PAFO

Figures 6 and 7 present the S-PAFO results at BOC and EOC, respectively. Unlike P-PAFO, S-PAFO targets restoration, so the required power adjustment is considerably slower. As shown in the figures, even with the UTSG model, both the reactor thermal power and the turbine thermal power track the demand closely at both burnup conditions.

Because S-PAFO requires a larger power ramp of up to ±5%Pr, the associated variation in the core inlet coolant temperature becomes inevitably larger than in the primary frequency control case. Thus, the core inlet temperature exceeds the RCS design limit by approximately 4 K at BOC and 1 K at EOC. The ASI exhibits a larger deviation than in P-PAFO, but the change remains modest and does not indicate any meaningful axial power-shape distortion during the transient.

Overall, the S-PAFO results indicate that PAFO can closely track secondary frequency-control demand in a large commercial PWR. At the same time, the inlet-temperature constraint emerges as the limiting factor, indicating that secondary frequency control performance is ultimately bounded by the RCS temperature design limits under the current APR1400 configuration.

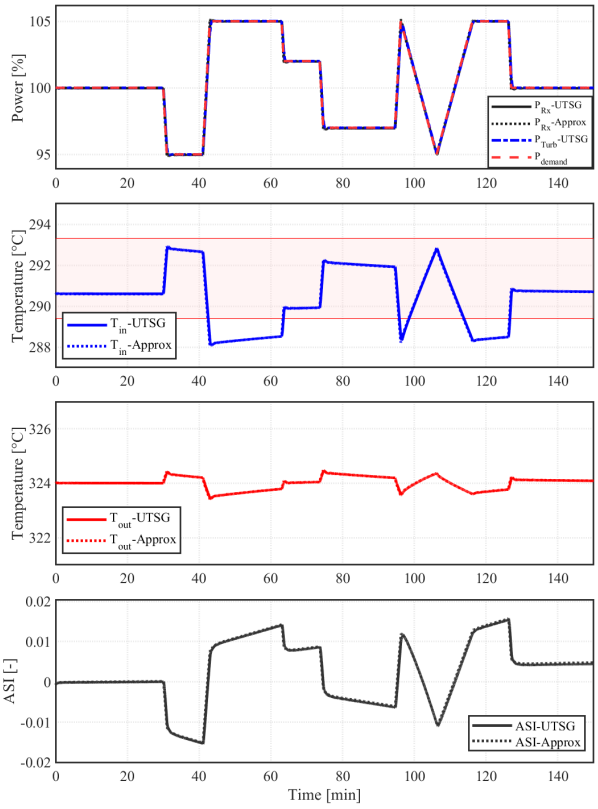

Figure 7 Simulation results of S-PAFO at EOC

4. Conclusions

This paper evaluates the feasibility of passively autonomous frequency operation in the APR1400 initial core for both primary and secondary frequency-control scenarios. The simulations show that a sufficiently negative moderator temperature coefficient is required for frequency control relying on inherent feedback alone.

PAFO is expected to be more favorable in an equilibrium core due to its more negative MTC. However, the results indicate that achieving successful PAFO under the most conservative condition, BOC, requires design improvements, such as increasing the allowable RCS inlet-temperature design limit or designing a low-boron core that provides a more negative MTC. In addition, limited use of control rods can be considered as a practical supplementary strategy when the inlet temperature exceeds the RCS design limit, particularly in the secondary frequency-control scenario.

Acknowledgements

This work was supported by the Innovative Small Modular Reactor Development Agency grant funded by the Korea government (MSIT) (No. RS-2024-00405419).

REFERENCES

[1] A. E. Abdelhameed, X. H. Nguyen, J. Lee, and Y. Kim, “Feasibility of passive autonomous frequency control operation in a Soluble-Boron-Free small PWR,” Annals of Nuclear Energy, vol. 116, pp. 319–333, 2018.

[2] Korea Electric Power Corporation (KEPCO) and Korea Hydro & Nuclear Power Co., Ltd. (KHNP), APR1400 Design Control Document Tier 2: Chapter 4, Reactor, Report No. APR1400-K-X-FS-14002-NP, Rev. 0, Dec. 2014.

[3] J. Leppänen, “Serpent – a continuous-energy Monte Carlo reactor physics burnup calculation code,” VTT Technical Research Centre of Finland, 2013.

[4] T. Oh, Y. Jeong, H. Khalefih, and Y. Kim, “Development and validation of multiphysics PWR core simulator KANT,” Nuclear Engineering and Technology, vol. 55, no. 6, pp. 2230–2245, 2023.

[5] Chaudri, K.S., Kim, J. and Kim, Y., 2019. Development and validation of a fast sub-channel code for LWR multiphysics analyses. Nuclear Engineering and Technology, 51(5), pp.1218-1230.

[6] Korea Electric Power Corporation (KEPCO) and Korea Hydro & Nuclear Power Co., Ltd. (KHNP), APR1400 Design Control Document Tier 2: Chapter 16, Technical Specifications, Report No. APR1400-K-X-FS-14002-NP, Rev. 0, Dec. 2014.